AGU PUBLICATIONS

Geophysical Research Letters

RESEARCH LETTER
10.1002/2016GL070454

Special Section:
The Arctic: An AGU Joint Special Collection

# Wind-driven mixing at intermediate depths in an ice-free Arctic Ocean

**Ben J. Lincoln[1], Tom P. Rippeth[1], Yueng-Djern Lenn[1], Mary Louise Timmermans[2], William J. Williams[3], and Sheldon Bacon[4]**

[1]School of Ocean Sciences, Bangor University, Bangor, UK, [2]Department of Geology and Geophysics, Yale University, New Haven, Connecticut, USA, [3]Fisheries and Oceans Canada, Institute of Ocean Sciences, Sidney, British Columbia, Canada, [4]National Oceanography Centre, Southampton, UK

**Abstract** Recent seasonal Arctic Ocean sea ice retreat is a major indicator of polar climate change. The Arctic Ocean is generally quiescent with the interior basins characterized by low levels of turbulent mixing at intermediate depths. In contrast, under conditions of reduced sea ice cover, there is evidence of energetic internal waves that have been attributed to increased momentum transfer from the atmosphere to the ocean. New measurements made in the Canada Basin during the unusually ice-free and stormy summer of 2012 show previously observed enhancement of internal wave energy associated with ice-free conditions. However, there is no enhancement of mixing at intermediate depths away from significant topography. This implies that contrary to expectations of increased wind-induced mixing under declining Arctic sea ice cover, the stratification in the central Canada Basin continues to suppress turbulent mixing at intermediate depths and to effectively isolate the large Atlantic and Pacific heat reservoirs from the sea surface.

**Key Points:**
- Ocean microstructure mixing measurements during a "perfect storm" of a relatively ice-free Arctic Ocean and an intense cyclone
- The ice-free ocean exhibits a strong response to the storm in the form of near-inertial oscillations
- The measurements show no enhanced mixing at the depths of the Atlantic and Pacific water in the Central Canada Basin

**Correspondence to:**
B. J. Lincoln,
ben.lincoln@bangor.ac.uk

**Citation:**
Lincoln, B. J., T. P. Rippeth, Y.-D. Lenn, M. L. Timmermans, W. J. Williams, and S. Bacon (2016), Wind-driven mixing at intermediate depths in an ice-free Arctic Ocean, *Geophys. Res. Lett.*, *43*, 9749–9756, doi:10.1002/2016GL070454.

Received 15 JUL 2016
Accepted 15 AUG 2016
Accepted article online 17 AUG 2016
Published online 17 SEP 2016



## 1. Introduction

The Arctic Ocean is generally regarded as quiescent, with very low levels of turbulent diapcynal mixing in the interior [*Padman*, 1995; *Fer*, 2009; *Lenn et al*., 2009; *Guthrie et al*., 2013]. At present, these low levels of mixing facilitate weak diapcynal heat fluxes, arising primarily from double diffusive convection, out of the intermediate depth Atlantic heat reservoir. Together with the intruding intermediate depth Pacific water the Atlantic water provides the main oceanic heat input to the Arctic Ocean. However, this state of very low mixing in the Arctic Ocean interior may be altered as a result of the recent decline in seasonal Arctic sea ice cover. Energetic internal waves have been observed in response to reduced sea ice cover, in both shelf sea [*Rainville and Woodgate*, 2009] and open Arctic Ocean locations [*Dosser et al*., 2014], which have been attributed to increased momentum transfer from the atmosphere to the ocean [*Giles et al*., 2012; *Martini et al*., 2014]. This has led to speculation that the future "seasonally ice-free" Arctic Ocean will see increased wind-induced ocean mixing [*Carmack and Melling*, 2011; *Martini et al*., 2014; *Martin et al*., 2014; *Tsamados et al*., 2014]. Subsequently, this hypothesized mixing could lead to a larger heat flux toward the sea surface from the temperature maxima of the intermediate depth Pacific and Atlantic origin water, potentially impacting sea ice thickness and extent.

The Arctic summer of 2012 was unique in several ways. A new record low sea ice extent was announced by the U.S. National Snow and Ice Data Center on 26 August, with the decline continuing for 23 more days before reaching a new record annual minimum on 18 September. The minimum areal extent in 2012 was 49% below the mean minimum (calculated over 1 day) for the period 1979–2000, with the largest new sea ice losses in the Canada Basin sector. Wind speeds are generally low during the Arctic summer; however, over the past 50 years, there has been a trend to increasing numbers of summer cyclones [*Sepp and Jaagus*, 2010]. In early August 2012, a storm formed over Siberia, and then moved across the Arctic Ocean, dying out over the Canadian Arctic 2 weeks later. Both the intensity and the longevity of the storm are atypical of the Arctic. The low central pressure (966 hPa) was the deepest of all 1618 cyclones recorded over the Arctic Ocean in August (in a record beginning in 1979), and the 13th lowest central pressure of any Arctic storm, regardless of month, recorded since 1979, leading to its designation as the "Great Arctic Cyclone of August 2012" [*Simmonds and Rudeva*, 2012]. The fluxing of subsurface oceanic heat to the surface by wind-induced turbulent mixing is implicated as a contributing factor to the additional ice melt which accompanied the Great Arctic Cyclone of 2012 [*Zhang et al*., 2013] resulting in the new record summer sea ice minimum of 2012.

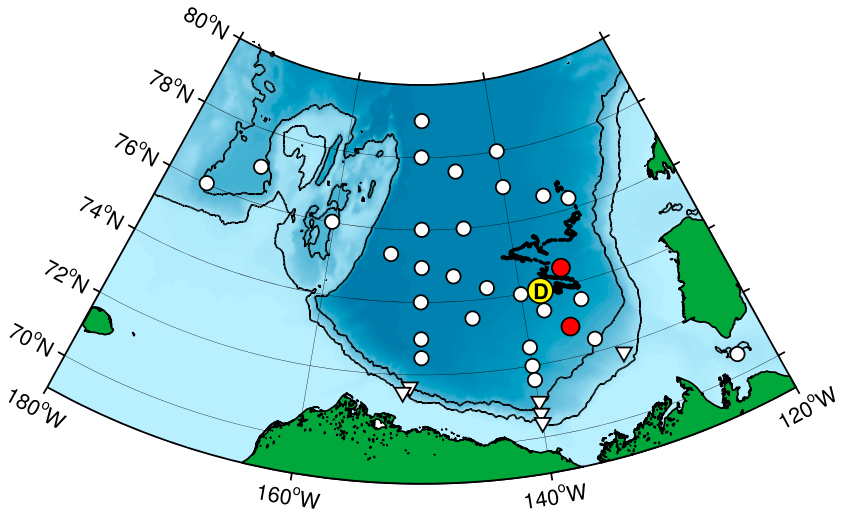


**Figure 1.** The Canada Basin, showing 2012 measurement locations. Mooring D: yellow circle at 74°N 140°W. VMP microstructure profiles are divided between those taken in the central basin (white circles) and those taken over significant topography (white triangles). The 200 m and 500 m isobaths are plotted in black to indicate the continental slope. ITP41 drift track (thick black line). Example temperature and salinity profiles plotted in Figure 2 are shown as red circles.

Multidecadal measurements of Arctic Ocean mixed layer characteristics show some variability of the mixed layer depths in response to wind forcing although they also suggest that density stratification is effective in suppressing the wind-driven mixing [*Peralta-Ferriz and Woodgate*, 2015; *Toole et al*., 2010]. Furthermore, observations in the Canada Basin indicate that, under typical wind conditions, the summer halocline may be eroded drawing near-surface heat upward, while the underlying Pacific and Atlantic layer heat remains untapped [*Timmermans*, 2015]. Key questions therefore arise as to what impact the enhanced atmosphere-ocean momentum transfer will have on wind-induced turbulent mixing at intermediate depth and hence on the fluxing of Pacific and Atlantic origin heat toward the sea surface, in the future seasonally ice-free Arctic Ocean.

Here we present new measurements made during the record-breaking ice-free conditions and unusually strong winds of August 2012, which led to an ideal natural experiment to test the impact of the wind on turbulent mixing at intermediate depths. The observations comprise a series of profiles of the rate of dissipation of turbulent kinetic energy (TKE) made in ice-free conditions in the Canada Basin during and following the passage of the Great Arctic Cyclone across that area. The new data are combined with long-term moored measurements to investigate whether this unique combination of an intense storm and newly open-water conditions drove enhanced diapycnal mixing at intermediate depths. In particular, we focus on the impact of the storm on mixing of heat toward the surface from the intermediate-depth Pacific and Atlantic water temperature maxima.

## 2. Methodology

A series consisting of 36 profiles of the rate of dissipation of turbulent kinetic energy, together with temperature and salinity, were made in the Canada Basin as part of the Beaufort Gyre Exploration Project (BGEP)/Joint Ocean Ice Studies (JOIS) research cruise during August 2012. The profiles were taken in open-water conditions at locations shown in Figure 1. The profiles were made with a loosely tethered free-fall velocity microstructure profiler (Rockland VMP500) and spanned the upper 500 m of the water column. The rate of dissipation of turbulent kinetic energy (TKE), $\varepsilon$, is calculated for depth bins of approximately 1 m under the assumptions of stationarity and homogeneity [*Lenn et al*., 2011]. Layer-averaged values of $\varepsilon$ and buoyancy frequency $N^2$ were calculated for the Pacific layer and upper Atlantic Water. Diapycnal heat fluxes are then estimated from these values by assuming a dissipation flux coefficient of $\Gamma = 0.2$. The layers over which the diapcynal heat fluxes are estimated are shown in Figure 2.

Supporting sea ice and oceanographic parameters are taken from the BGEP mooring D, which was located in the Eastern Beaufort Sea at 74.0°N 140°W, in water about 3800 m deep. The measurements presented

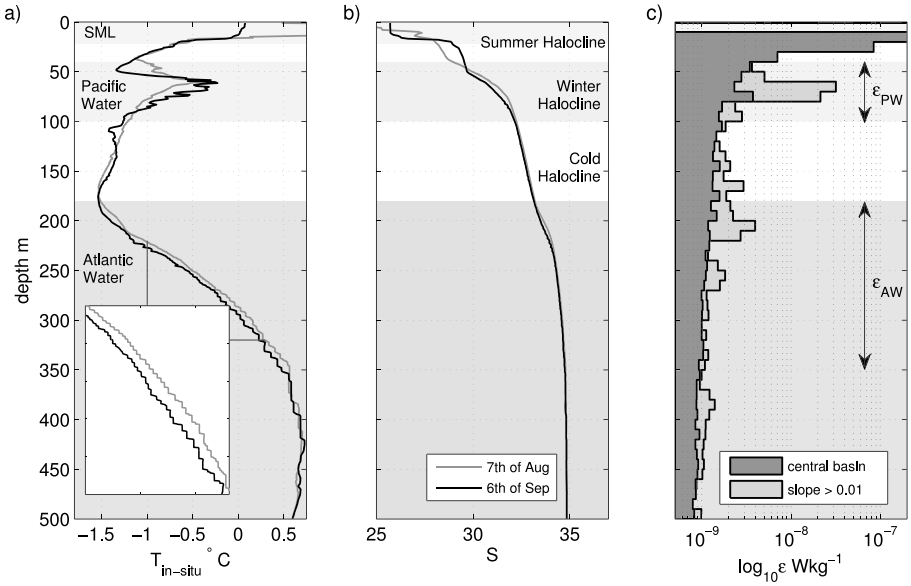


**Figure 2.** Profiles of water column structure and the rate of dissipation of TKE ($\varepsilon$). Profiles of (a) temperature and (b) salinity from 7 August 2012 (grey) and 6 September 2012 (black) during the JOIS hydrographic expedition in the central Canada Basin. (c) The mean $\varepsilon$ profiles for the central Canada Basin (formed from the 30 VMP profiles made over a sea bed slope $< 0.01$) and over the continental slope (the six profiles where bed slope $> 0.01$). The levels of the different water masses and interfaces named in the text are shown on Figures 2a and 2b, respectively, while the respective integration range for the calculation of the mean Pacific water and the section of the water column separating the cold Halocline from the Atlantic water are indicated on Figure 2c.

were made using instruments mounted on the top flotation buoy on the mooring located ~30 m below the sea surface. They consist of an Upward Looking Sonar (ULS) which measured the thickness of the ice beneath the sea surface at the mooring. The ice draft values are daily means of these measurements calculated following *Krishfield et al*. [2014]. An upward looking 600 kHz Acoustic Doppler Current Profiler (ADCP), also mounted in the buoy, recorded hourly current profiles in the surface waters over a range from 28 m to 3 m below the surface during summer, although this is reduced in winter due to acoustic reflections from the sea ice.

The amplitude of inertial currents was calculated from the ADCP data using a least squares fitting method at the local inertial period, $T_I = 12/\sin\phi_L = 12.48$ h (where $\phi_L$ is the mooring latitude), to 13 h sections of mean currents from two different depth ranges. The range 3–15 m was chosen to represent the SML, while mean currents below 20 m were used to quantify currents below the stratified base of the SML. The depth range approximation is supported by density profiles collected from the mooring site during August, and visual examination of the velocity structure suggests that it is valid during the summer months, when the SML is generally less than 20 m thick.

Further information on the internal wave field is obtained from an Ice-Tethered Profiler (ITP no. 41) [*Krishfield et al*., 2008] which had been deployed in October 2010 and collected two vertical profiles of temperature and salinity per day, at 06:00 and 12:00 between 7 and 750 m depth by means of a conductivity-temperature-depth profiler suspended on a wire from beneath an ice floe. The ITP sampling schedule is designed to balance endurance with the need to eliminate aliasing of motions at the semidiurnal tidal and inertial periods [*Dosser et al*., 2014]. To overcome this bias a least squares fitting method [*Dosser et al*., 2014] using complex demodulation was employed on ITP profiles between January and August 2012 to estimate the isopycnal displacements at the inertial frequency. These are calculated over the depth range 50–200 m, and scaled to account for vertical variation in stratification. During the period of interest, the ITP drifted east then south and as a result was located very close to mooring D in August 2012 (Figure 1). During and after the cyclone, only partial ITP profiles were returned as the automated profiler had difficulty climbing the wire during times of anomalously fast drift, and as a consequence, fewer estimates of internal wave amplitude were possible.

## 3. Results

The profiles of temperature and salinity for early August and September 2012 reveal five distinct and well-known layers in the upper 500 m of the water column (Figure 2a). The SML, extending from the surface to between 5 and 20 m has low salinity (≈25–26) and a temperature which varies from 5°C in the southern basin to freezing temperature (≈ −1.8°C in the north). This overlies several layered water masses which comprise the halocline. In the profiles shown, a cooler layer lies below the base of the surface layer (i.e., the summer halocline); this layer is a remnant of the previous winter's mixed layer and extends to about 50 m. Next, a layer of warmer (by ≈1.0°C) Pacific origin water (PW) lies between 50 and 100 m depth, with cooler halocline waters between 100 and 200 m. Below about 200 m, the temperature increases with depth to the warm core (~0.5°C) of the Atlantic origin water (AW) located at around 400 m depth. Thermohaline staircases are evident across the section of the water column separating the AW from the cold halocline above, in all profiles taken in the central Canada Basin. Such phenomena are commonly observed in the Arctic Ocean where the water column exhibits bulk gradients in temperature and salinity that both increase with depth [*Padman and Dillon*, 1988; *Timmermans et al*., 2008; *Fer*, 2009; *Lenn et al*., 2009]. Staircases arise as a consequence of low levels of turbulent mixing coupled with differing rates of molecular diffusion for heat and salt [*Ruddick and Gargett*, 2003]. In contrast, the thermohaline staircase is absent in the six VMP profiles taken over the continental slope, despite stratification favorable for double diffusion, thus suggesting higher levels of turbulent mixing at intermediate depth at these locations.

Mean profiles of the rate of dissipation of TKE ($\varepsilon$) are calculated for the central basin (i.e., the mean of 30 profiles where the sea bed slope is $<0.01$) and over the continental slope (i.e., the mean of six profiles where sea bed gradient is $>0.01$; see Figure 2). In the central basin, below the surface mixed layer, $\varepsilon$ declines and is close to the instrument noise level ($5\times10^{-10}\,\mathrm{W\,kg^{-1}}$) except in the PW layer where there is a small enhancement. In contrast, $\varepsilon$ is enhanced over sloping topography in the layers of strong stratification corresponding to the strong gradients associated with the PW and AW. Within the PW layer, $\varepsilon$ rises by an order of magnitude, from $2\times10^{-9}\,\mathrm{W\,kg^{-1}}$ in the central basin to $2\times10^{-8}\,\mathrm{W\,kg^{-1}}$ over the continental slope. There is also a more modest rise over the continental slope when compared to the central basin, $3\times10^{-9}\,\mathrm{W\,kg^{-1}}$ compared to $1\times10^{-9}\,\mathrm{W\,kg^{-1}}$ across the region of the water column separating the AW core from the cold halocline.

To set these measurements into a wider context we present observations of the seasonal variability in sea ice conditions and upper ocean currents during spring and summer 2012, at a local mooring position (mooring D in Figure 3). In March, sea ice cover was close to 100% and the ice was near stationary. Through April and May, the dense sea ice was observed to drift at a rate proportional to the wind strength: the ratio of ice to wind speed was 2%, which is consistent with previously reported values [e.g., *Thorndike and Colony*, 1982]. The ice began to fracture in late May, with about 5% open water observed throughout June. As the season progressed, the sea ice continued to decline and the mooring location became ice-free by the end of the first week of August. The ice-free conditions persisted for almost 3 months, with ice reappearing in late October.

The disappearance of the sea ice in early August coincided with the period of substantially elevated winds (Figure 3a) over the area associated with the passage of the Great Arctic Cyclone. Overall, the ice-free conditions of August to October coincided with an unusually windy period when the daily mean surface wind stress (from the National Center for Environmental Prediction, NCAR, reanalysis) was ~70% higher than the mean for the remainder of 2012, and unprecedented for August since the National Centers for Environmental Prediction (NCEP) reanalysis time series began in 1979 [*Simmonds and Rudeva*, 2012].

A strong oceanic response to the ice-free conditions is evident in the upper water column currents (Figure 3c), which showed an order-of-magnitude increase in horizontal velocities coincident with the thinning and breaking of the sea ice in July. This is highlighted by the variability in the inertial currents over the two chosen depth ranges, which is shown in Figure 3c. Early in the year, near-inertial currents are small, 0.01–0.03 $\mathrm{m\,s^{-1}}$. They begin to increase in June, with a more substantial increase in July coinciding with the breakup and subsequent disappearance of the sea ice. At this time the near-inertial current speed increased from 0.05 $\mathrm{m\,s^{-1}}$ to 0.25 $\mathrm{m\,s^{-1}}$, corresponding to a 25-fold increase in the horizontal kinetic energy in the ocean surface mixed layer since the spring. The largest near-inertial currents ($>0.2\,\mathrm{m\,s^{-1}}$) were found during late July and early August when ice concentration was low ($<50\%$), and continuing to decline, with an ice thickness $<1$ m. This result is consistent with those of *Martin et al*. [2014], who showed that an optimum concentration of sea ice can lead to an enhancement of the efficiency of momentum transfer from the

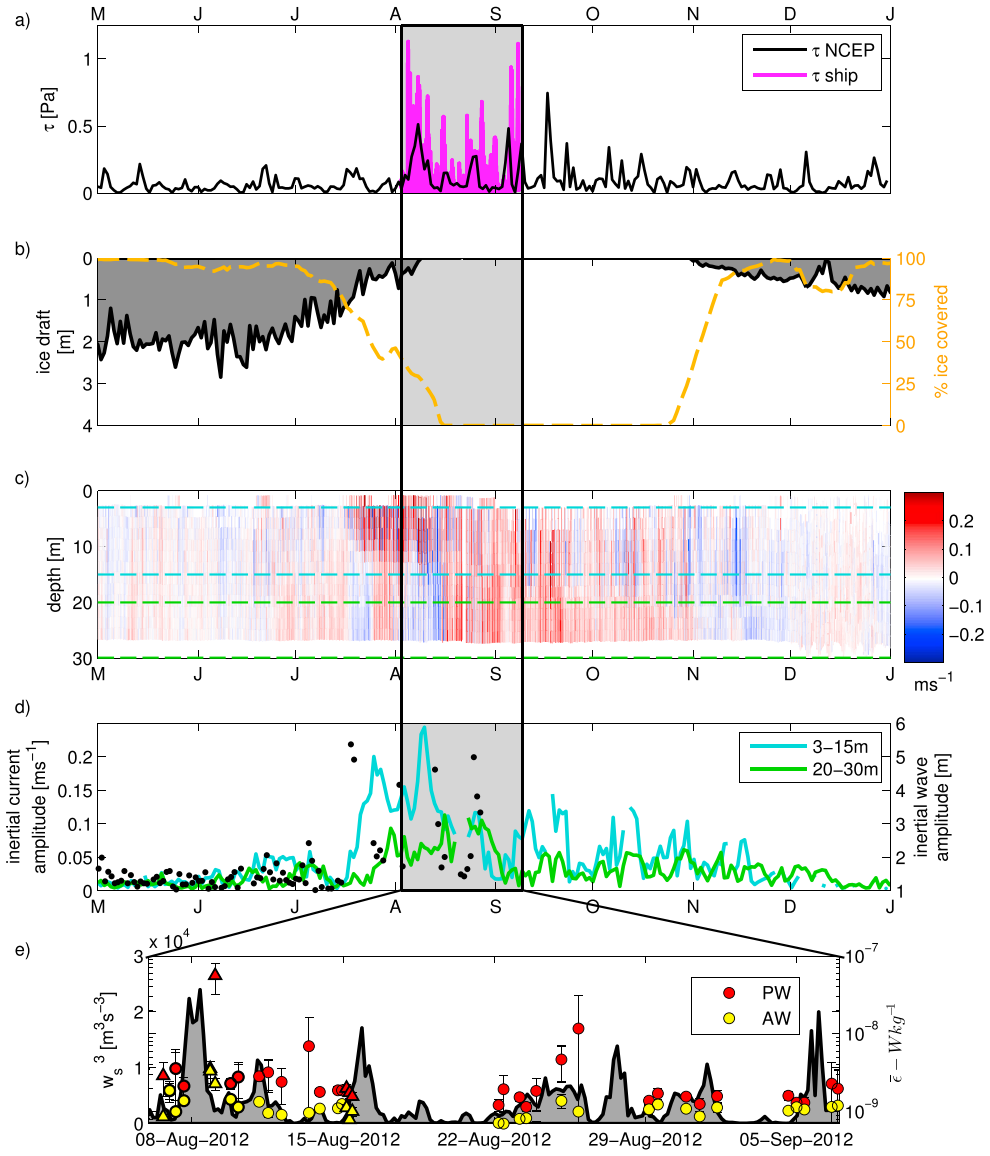


**Figure 3.** Wind stress, sea ice, and current observations from the Eastern Canada Basin in 2012 (at mooring D in Figure 1) accompanied by TKE dissipation measurements from across the region during August 2012 when inertial internal wave energy levels peaked. (a) Wind stress calculated from NCEP reanalysis daily values (black) and from ship measurements (magenta). (b) Mean daily ice draft measured by upward looking sonar (shaded area) and percent of time that the mooring site was ice covered (orange dashed line). (c) Velocity data measured by upward looking acoustic current meter. Blue and green dashed lines indicate depth ranges 3–15 m and 20–30 m for the fits plotted in Figure 3d. (d) Amplitude of inertial period currents calculated by least squares fit to 13 h sections of velocity data over the depth ranges indicated in Figure 3c. Black dots indicate the inertial period internal wave amplitude calculated from ITP data over the depth range 50–200 m. (e) An expanded section covering only the period of the microstructure measurements (August 2012) showing the profile mean Pacific water (40–100 m), $\varepsilon_{PW}$, in red and the section of the water column separating the Cold Halocline from the Atlantic water (180–240 m), $\varepsilon_{AW}$, in yellow. The TKE dissipation rates together with the cube of the wind speed (shaded grey). Profiles taken over the continental slope (i.e., slope $> 0.01$) are plotted as triangles and those in the central Canada Basin as circles (slope $< 0.01$). In both cases the variability is indicated as the 95% confidence interval. Ship measured wind speed cubed is plotted in grey as a proxy for the rate of kinetic energy transfer from the atmosphere to the ocean surface layer. The period of the microstructure measurements is shown in Figures 3a–3c as a grey-shaded area.

atmosphere to the ocean. Figure 3d shows that the inertial currents are generally larger over the range 3–15 m than over 20–30 m layers with the relative changes between the two likely due to changes in stratification resulting from buoyancy input to the surface mixed layer due to summer freshening and warming. Concurrent measurements from the ITP between January and August 2012 show that the mean resultant

inertial internal wave amplitude over the depth range 50–200 m was found to be correlated to the near-inertial currents in the upper part of the water column ($r = 0.62$) implying that the near-inertial currents observed at intermediate depths are related to those observed close to the surface. This observation is consistent with *Dosser and Rainville* [2016], who show that internal inertial wave activity at depth peaks annually during the ice-free summer period and that the largest amplitude waves over the available 10 year record occurred during the summer of 2012.

Time series of the profile average $\varepsilon$ for the depth of the PW layer and the region of the water column separating the AW core from the cold halocline are shown in Figure 3e alongside the cube of the wind speed measured from the ship ($w_s^3$), to represent the rate of kinetic energy transfer from the wind. Mean AW dissipation rates are ~$6 \times 10^{-10}$ W kg$^{-1}$, only just above the instrument noise level, while within the PW layer, dissipation rates are up to 2 orders of magnitude higher, at $2 \times 10^{-9}$ to $6 \times 10^{-8}$ W kg$^{-1}$. The profiles showing significantly enhanced $\varepsilon$ at intermediate depths are found over the continental slope indicating topographic effects may also be important (Figure 2c). However, there is no significant relationship ($r < 0.1$) between $w_s^3$ and either the PW or the AW layer-averaged $\varepsilon$ in the central basin. The heat fluxes resulting from the observed $\varepsilon$ are modest, with an upward heat flux of $0.7 \pm 0.4$ W m$^{-2}$ from the PW in the central basin similar to those reported under ice by *Shaw et al*. [2009]. PW heat fluxes over the continental slope are elevated to as much as 6 W m$^{-2}$ which is comparable to PW heat flux estimates over rough topography under ice [*Shaw et al*., 2009]. The average heat flux from the AW into the overlying cold halocline is estimated to be $0.14 \pm 0.03$ W m$^{-2}$ in the central basin, with a modest rise to $0.24 \pm 0.1$ W m$^{-2}$ over the slope. These fluxes are comparable to reported fluxes arising from double diffusion in this region [*Padman and Dillon*, 1987; *Timmermans et al*., 2008] but are considerably smaller than the AW heat fluxes reported for continental slope region north of Svalbard of about 20 W m$^{-2}$ [*Padman and Dillon*, 1991; *Rippeth et al*., 2015].

## 4. Discussion

The new observations presented offer a unique glimpse of an aspect of the likely mixing regime in the future seasonally ice-free central Arctic Ocean. Current meter time series show an order-of-magnitude increase in near-inertial current velocities, in response to the breakup and disappearance of the sea ice, with a consequent increase in kinetic energy of 2 orders of magnitude. This result is consistent with previous observations [*Rainville and Woodgate*, 2009; *Lenn et al*., 2011; *Dosser et al*., 2014; *Martini et al*., 2014] which have in turn led to speculation that decreasing ice cover will lead to increased wind mixing [*Rainville and Woodgate*, 2009; *Carmack and Melling*, 2011]. However, despite the open water, the anomalously strong atmospheric forcing and the consequent enhanced levels of internal wave energy, the directly observed mixing levels at intermediate depths within the central Canada Basin remain low leading to a diapcynal heat flux from the Atlantic water of $0.14 \pm 0.03$ W m$^{-2}$ and comparable to under-ice estimates acquired under sea ice cover in the Canada [*Padman & Dillon*, 1987; *Lique et al*., 2014] and Eurasian [*Lenn et al*., 2009; *Sirevaag and Fer*, 2012; *Fer*, 2014] basins of the Arctic Ocean.

Furthermore, the thermohaline staircase separating the core of the Atlantic water from the cold halocline above was observed to be a persistent feature in all profiles taken in the central Canada Basin (Figure 2a). The persistence of the staircase indicates the absence of significant shear-driven turbulent mixing at these depths over the period of interest as turbulence would disrupt the well-formed step structure. For example, *Bebieva and Timmermans* [2016] found no staircase at the flanks of an AW eddy where geostrophic shear leads to higher mixing; they estimated that diapycnal diffusivities are an order of magnitude larger where the staircase is absent compared to measurements several kilometers away that are characterized by a well-formed staircase. *Timmermans et al*. [2008] demonstrated the persistence and lateral coherency of individual mixed layers in the staircase over the entire central Canada Basin, consistent with enhanced mixing events being rare. It is therefore reasonable to assume that the sustained presence of the staircase fine structure in these new observations implies that the very low levels of turbulence derived from the synoptic microstructure observations are representative of the central Canada Basin mixing environment, over the duration of the Great Arctic Cyclone of 2012, at these depth levels.

These new result imply that, despite the exceptional loss of sea ice cover in summer 2012, the stratification in the central Canada Basin is presently sufficiently strong to isolate the intermediate-depth heat reservoir from the direct impact of enhanced mixing resulting from increased momentum transfer from the wind. These

new results therefore further highlight the key role of stratification in isolating the intermediate depths from wind-driven mixing. In a future seasonally ice-free Arctic Ocean, stratification in the surface mixed layer and cold halocline will likely increase in response to increased freshwater runoff coupled with an increased seasonal sea ice melt volume; in this setting, the competing influences of enhanced internal wave stresses and stratification barriers to turbulent mixing at intermediate depths are likely to be complicated.

Finally, the new results also provide some evidence of the key role of topography and so point to the localized nature of enhanced diapcynal mixing and oceanic heat fluxes toward the sea surface [*Padman and Dillon*, 1991; *Rippeth et al*., 2015]. While reduced sea ice extent will likely lead to the increased transfer of momentum from the atmosphere to the ocean [e.g., *Giles et al*., 2012] and higher near-inertial energy [e.g., *Pinkel*, 2005], our results indicate that enhanced turbulence will be largely restricted to the steeper topography of the basin margins.

**Acknowledgments**
VMP Turbulence data collection and analysis were funded through the UK Natural Environmental Research Council (NERC) TEA-COSI Consortium, NE/I029072/1 (PI SB). VMP technical support was ably provided by Ben Powell. The authors wish to thank the Captain, crew, and participating scientists of the CCGS *Louis St-Laurent* for their cooperation during the data collection. Hydrographic and mooring data were collected and made available by the Beaufort Gyre Exploration Program based at the Woods Hole Oceanographic Institution (http://www.whoi.edu/beaufortgyre) in collaboration with researchers from Fisheries and Oceans Canada at the Institute of Ocean Sciences. The Ice-Tethered Profiler data were collected and made available by the Ice-Tethered Profiler Program based at the Woods Hole Oceanographic Institution [*Krishfield et al*. 2008; *Toole et al*. 2011]. BGEP ice draft data were provided by Rick Krishfield [*Krishfield et al*., 2014]. Daily wind-stress values were provided by the NCAR-NCEP reanalysis product, available here: http://www.esrl.noaa.gov/psd/data/gridded/data.ncep.reanalysis.derived.surfaceflux.html. Access to the microstructure data used in the paper may be requested from the British Oceanographic Data Centre, National Oceanography Centre, Liverpool (http://www.bodc.ac.uk). Hydrographic and mooring data were collected and made available by the Beaufort Gyre Exploration Program based at the Woods Hole Oceanographic Institution (http://www.whoi.edu/beaufortgyre). S.B., T.P.R., Y.D.L., W.J.W., and B.J.L. planned and directed the VMP measurements presented in this paper. B.J.L., T.P.R., Y.D.L., and M.L.T. analyzed and interpreted the hydrographic and mooring data presented. B.J.L. wrote the first draft of the paper with all authors contributing to its revision.

## References

Bebieva, Y., and M.-L. Timmermans (2016), An examination of double-diffusive processes in a mesoscale eddy in the Arctic Ocean, *J. Geophys. Res. Oceans*, *121*, 457–475, doi:10.1002/2015JC011105.0485(2004)034<1679:SVODMA>2.0.CO;2.
Carmack, E., and H. Melling (2011), Cryosphere: Warmth from the deep, *Nat. Geosci.*, *4*, 7–8, doi:10.1038/ngeo1044.
Dosser, H. V., and L. Rainville (2016), Dynamics of the changing near-inertial internal wave field in the Arctic Ocean, *J. Phys. Oceanogr.*, *46*(2), 395–415, doi:10.1175/JPO-D-15-0056.1.
Dosser, H. V., L. Rainville, and J. M. Toole (2014), Near-inertial internal wave field in the Canada Basin from ice-tethered profilers, *J. Phys. Oceanogr.*, *44*, 413–426, doi:10.1175/JPO-D-13-0117.1.
Fer, I. (2009), Weak vertical diffusion allows maintenance of cold halocline in the central Arctic, *Atmos. Ocean Sci. Lett.*, *2*, 148–152.
Fer, I. (2014), Near-inertial mixing in the central Arctic Ocean, *J. Phys. Oceanogr.*, *44*, 2031–2049, doi:10.1175/JPO-D-13-0133.1.
Giles, K. A., S. W. Laxon, A. L. Ridout, D. J. Wingham, and S. Bacon (2012), Western Arctic Ocean freshwater storage increased by wind-driven spin-up of the Beaufort Gyre, *Nat. Geosci.*, *5*, 194–197, doi:10.1038/ngeo1379.
Guthrie, J. D., J. H. Morison, and I. Fer (2013), Revisiting internal waves and mixing in the Arctic Ocean, *J. Geophys. Res. Oceans*, *118*, 3966–3977, doi:10.1002/jgrc.20294.
Krishfield, R., J. M. Toole, A. Proshutinsky, and M.-L. Timmermans (2008), Automated Ice-Tethered profilers for sea water observations under pack ice in all seasons, *J. Atmos. Oceanic Technol.*, *25*, 2091–2095.
Krishfield, R., A. Proshutinsky, K. Tatekeyama, W. J. Williams, E. C. Carmack, F. A. McLaughlin, and M.-L. Timmermans (2014), Deterioration of perennial sea ice in the Beafort Gyre from 2003 to 2012 and its impact on the oceanic frewshwater cycle, *J. Geophys. Res. Oceans*, *119*, 1271–1305, doi:10.1002/2013JC008999.
Lenn, Y. D., et al. (2009), Vertical mixing at intermediate depths in the Arctic boundary current, *Geophys. Res. Lett.*, *36*, L05601, doi:10.1029/2008GL036792.
Lenn, Y.-D., T. P. Rippeth, C. P. Old, S. Bacon, I. Polyakov, V. Ivanov, and J. Hölemann (2011), Intermittent intense turbulent mixing under ice in the Laptev Sea continental shelf, *J. Phys. Oceanogr.*, *41*, 531–547.
Lique, C., J. D. Guthrie, M. Steele, A. Proshutinsky, J. H. Morison, and R. Krishfield (2014), Diffusive vertical heat flux in the Canada Basin of the Arctic Ocean inferred from moored instruments, *J. Geophys. Res. Oceans*, *119*, 496–508, doi:10.1002/2013JC009346.
Martin, T., M. Steele, and J. Zhang (2014), Seasonality and long-term trend of Arctic Ocean surface stress in a model, *J. Geophys. Res. Oceans*, *119*, 1723–1738, doi:10.1002/2013JC009425.
Martini, K. I., H. L. Simmons, C. A. Stoudt, and J. K. Hutchings (2014), Near-inertial internal waves and sea ice in the Beaufort Sea, *J. Phys. Oceanogr.*, *44*, 2212–2234, doi:10.1175/JPO-D-13-0160.1.
Padman, L. (1995), Small-scale physical processes in the Arctic Ocean, in *Arctic Oceanography: Marginal Ice Zones and Continental Shelves*, *Coastal and Estuarine Studies*, vol. 49, edited by W. O. Smith and J. Grebmeier, AGU, Washington, D. C.
Padman, L., and T. M. Dillon (1987), Vertical heat fluxes through the Beaufort Sea thermohaline staircase, *J. Geophys. Res.*, *92*, 10,799–10,806, doi:10.1029/JC092iC10p10799.
Padman, L., and T. M. Dillon (1988), On the horizontal extent of the Canada Basin thermohaline steps, *J. Phys. Oceanogr.*, *18*, 1458–1462.
Padman, L., and T. M. Dillon (1991), Turbulent mixing near the Yermak Plateau during the Coordinated Eastern Arctic Experiment, *J. Geophys. Res.*, *96*, 4769–4782, doi:10.1029/90JC02260.
Peralta-Ferriz, C., and R. A. Woodgate (2015), Seasonal and interannual variability of pan-Arctic surface mixed layer properties from 1979 to 2012 from hydrographic data, and the dominance of stratification for multiyear mixed layer depth shoaling, *Prog. Oceanogr.*, *134*, 19–53, doi:10.1016/j.pocean.2014.12.005.
Pinkel, R. (2005), Near-inertial wave propagation in the western Arctic, *J. Phys. Oceanogr.*, *35*, 645–665.
Rainville, L., and R. A. Woodgate (2009), Observations of internal wave generation in the seasonally ice-free Arctic, *Geophys. Res. Lett.*, *36*, L23604, doi:10.1029/2009GL041291.
Rippeth, T. P., B. J. Lincoln, Y.-D. Lenn, J. A. Mattias Green, A. Sundfjord, and S. Bacon (2015), Tide-mediated warming of Arctic halocline by Atlantic heat fluxes over rough topography, *Nat. Geosci.*, 5–8, doi:10.1038/ngeo2350.
Ruddick, B., and A. E. Gargett (2003), Oceanic double-infusion: Introduction, *Prog. Oceanogr.*, *56*, 381–393, doi:10.1016/S0079-6611(03)00024-7.
Sepp, M., and J. Jaagus (2010), Changes in the activity and tracks of Arctic cyclones, *Clim. Change*, *105*, 577–595, doi:10.1007/s10584-010-9893-7.
Shaw, W. J., T. P. Stanton, M. G. McPhee, J. H. Morison, and D. G. Martinson (2009), Role of the upper ocean in the energy budget of Arctic sea ice during SHEBA, *J. Geophys. Res.*, *114*, C06012, doi:10.1029/2008JC004991.
Simmonds, I., and I. Rudeva (2012), The Great Arctic cyclone of August 2012, *Geophys. Res. Lett.*, *39*, L23709, doi:10.1029/2012GL054259.
Sirevaag, A., and I. Fer (2012), Vertical heat transfer in the Arctic Ocean: The role of double-diffusive mixing, *J. Geophys. Res.*, *117*, C07010, doi:10.1029/2012JC007910.
Thorndike, A. S., and R. Colony (1982), Sea ice motion in response to geostrophic winds, *J. Geophys. Res.*, *87*, 5845–5852, doi:10.1029/JC087iC08p05845.

Timmermans, M.-L. (2015), The impact of stored solar heat on Arctic sea ice growth, *Geophys. Res. Lett.*, *42*, 6399–6406, doi:10.1002/2015GL064541.

Timmermans, M.-L., J. Toole, R. Krishfield, and P. Winsor (2008), Ice-Tethered Profiler observations of the double-diffusive staircase in the Canada Basin thermocline, *J. Geophys. Res.*, *113*, C00A02, doi:10.1029/2008JC004829.

Toole, J. M., M.-L. Timmermans, D. K. Perovich, R. A. Krishfield, A. Proshutinsky, and J. A. Richter-Menge (2010), Influences of the ocean surface mixed layer and thermohaline stratification on Arctic Sea ice in the central Canada Basin, *J. Geophys. Res.*, *115*, C10018, doi:10.1029/2009JC005660.

Toole, J. M., R. Krishfield, M.-L. Timmermans, and A. Proshutinsky (2011), The Ice-Tethered Profiler: Argo of the Arctic, *Oceanography*, *24*, 126–135.

Tsamados, M., D. L. Feltham, D. F. Schroeder, S. L. Farrell, N. T. Kurtz, and S. W. Laxon (2014), Impact of atmospheric and oceanic form drag parameterization on simulations of Arctic sea ice, *J. Phys. Oceanogr.*, *44*, 1329–1353.

Zhang, J., R. Lindsay, A. Schweiger, and M. Steele (2013), The impact of an intense summer cyclone on 2012 Arctic sea ice retreat, *Geophys. Res. Lett.*, *40*, 720–726, doi:10.1002/grl.50190.